24th INTERNATIONAL CONGRESS ON SOUND AND VIBRATION
23–27 July 2017, London

ICSV24
23-27JULY 2017
LONDON CALLING

INVESTIGATION OF AEROACOUSTICS PROBLEMS USING A DISCONTINUOUS GALERKIN SPECTRAL ELEMENT METHOD

Bao Zhenzhong and Qin Guoliang

Xi'an Jiaotong University, Department of Fluid Mechanics and Engineering, Xi'an 710049, P R China

email: onebao@stu.xjtu.edu.cn

Needs of accurate and efficient numerical solvers in CAA have motivated the development of low-dispersion and low-dissipation schemes, the capabilities of the high resolution discontinuous Galerkin spectral element method for the simulation of aeroacoustic problems are investigated in the present work. The linearized Euler equation is discretizationed by discontinuous Galerkin spectral element method in space and the classical fourth order Runge-Kutta method in time marching, the characteristic absorbing boundary condition is adopted too, and the Riemann's problem presented in linearized Euler equation is tackled by a HLL numerical flux. Two dimensional example of a convected isentropic vortex is computed with three different meshes to demonstrate the high accuracy of the proposed method. The exponential convergence can be obtained for a fixed mesh and increasing local polynomial order, then it is proved that the discontinuous Galerkin spectral element method has the h/p convergence property. The sound scattering by a cylinder is also simulated and the numerical results are compared with the analytical data. It is shown that the numerical results agree well with the analytical data. The paper can provide a theoretical foundation for solving the computational aeroacoustics problems with a high order of accuracy.

Key words: computational aeroacoustics, discontinuous Galerkin method, spectral element method, linearized Euler equation, exponential convergence

1. Introduction

With the rapid advancement of high-speed computational capability, the Computational fluid dynamics (CFD) have been used widely in science and engineering. However, traditional CFD methods that are aimed at dealing with fluid dynamics problems numerically cannot meet the demand of aeroacoustic problems. Therefore, the CAA (Computational Aero-acoustic) have been developed since 1990s [1-3].

Needs of accurate and efficient numerical solvers in CAA have motivated the development of low-dispersion and low-dissipation schemes. Discontinuous Galerkin spectral element method (DG-SEM) [4,5] is the combining of the discontinuous Galerkin method [6] and spectral element method (SEM) [7], so which features the goodness of two technologies. The spectral element method is an advanced implementation of the finite element method in which the solution over each element is expressed in terms of a priori unknown values at carefully selected spectral nodes. The advantage of the SEM is that stable solution algorithms and high accuracy can be achieved with a low number of elements. Additionally, SEM is also very well suited to deal with complicated geometries. The DG methods can easily handle adaptivity strategies, and since the elements are discontinuous, the resulting mass matrix is block-diagonal, so the DG methods can be highly parallelized.

So far DG-SEM has not been widely used in CAA area. The dispersion and dissipation properties of the Gauss and Gauss-Lobatto DG-SEM have been well studied by means of theory (can be found in [5]). Muhammed *et al*. [8] applied the DG-SEM for studying the sound generate and acoustic feedback mechanisms at a side-view mirror by solving the fully compressible Navier-Stokes equations, however, the computational cost is very expensive. David *et al*. [9] researched the trailing edge noise for airfoil flows at medium Reynolds numbers, and this demonstrated the capabilities of DG-SEM for the accurate numerical simulation of the complex aeroacoustic problems. In this work, an investigation is conducted in order to evaluate the scheme order and acoustic propagation problems.

The remainder of this paper is organized as follows. In Section 2 we provide a description of the linearized Euler equation for acoustic propagation problems, and the governing equation will then be discretized by DG-SEM in space and classical fourth order Runge-Kutta method in time marching. In Section 3, the isentropic vortex propagation case and the acoustic wave scatting by a circular cylinder are investigated in detail. Finally, Section 4 contains the conclusions of our work.

2. Theory

2.1 Governing equation

In theory flow variables and acoustic variables are all governed by the fully compressible Navier-Stokes equations. However, given the large computational cost, the simplified solution of acoustic propagation problems can be numerically simulated by solving the LEE.

LEE in conservative form can be written as:

$$\frac{\partial \boldsymbol{U}}{\partial t}+\nabla\cdot\vec{\boldsymbol{F}}\left(\boldsymbol{U}\right)=\boldsymbol{S}\,, \tag{1}$$

where $\vec{\boldsymbol{F}}=\left(\boldsymbol{F}_1\left(\boldsymbol{U}\right),\ \boldsymbol{F}_2\left(\boldsymbol{U}\right)\right)^T$,and $\boldsymbol{U}$ is the vector of conservative variable, $\boldsymbol{F}_1\left(\boldsymbol{U}\right)$, $\boldsymbol{F}_2\left(\boldsymbol{U}\right)$ are the two-dimensional flux vectors, respectively. $\boldsymbol{S}$ is a source term, which can contain an initial condition of a pressure disturbance, or a possible unsteady sources in the flow field. The corresponding expression is as follows,

$$\begin{aligned}
&\boldsymbol{U}=\left(\rho,\rho u,\rho v,E\right)^T,\\
&\boldsymbol{F}_1\left(\boldsymbol{U}\right)=\left(\rho u,p+\rho u^2,\rho uv,u\left(E+p\right)\right)^T,\\
&\boldsymbol{F}_2\left(\boldsymbol{U}\right)=\left(\rho v,\rho uv,p+\rho v^2,v\left(E+p\right)\right)^T.
\end{aligned} \tag{2}$$

Here ρ is the density, P is the pressure, u,v are the Cartesian velocity components and E is the total energy. The system is completed by the following equation of state for a perfect gas,

$$\mathrm{p}=\left(\gamma-1\right)\left(\mathrm{E}-\frac{1}{2}\rho\left(\mathrm{u}^2+\mathrm{v}^2\right)\right), \tag{3}$$

where γ is the ratio of specific heats.

2.2 Spatial and time discretization

In the present paper, we adopt the DG-SEM to discretize the governing equation in space. First, subdivide the domain Ω into N_{el} non-overlapping elements, Each spectral element is mapped into a standard element [-1,1]. Trial functions $U_h=\sum_{m=0}^{P}u_m\left(t\right)\phi_m\left(x,y\right)$, where P is the interpolation order. One dimensional basis functions is defined in the standard element by the following:

$$\phi_p(\xi)=\begin{cases}\dfrac{1-\xi}{2}, & p=0,\\ \left(\dfrac{1-\xi}{2}\right)\left(\dfrac{1+\xi}{2}\right)P_{p-1}^{1,1}(\xi), & 0<p<P,\\ \left(\dfrac{1+\xi}{2}\right), & p=P.\end{cases} \tag{4}$$

where $P_{p-1}^{1,1}(\xi)$ is 1,1 Jacobi polynomials.

Then, with the common Galerkin approach the test functions w_l are chosen identical to the basis functions, and by integrating over the reference element and using a spatial integration by parts we obtain the weak formulation of DG-SEM formulation.

$$\frac{d}{dt}\int_{e_i}\boldsymbol{U}w_l de_i+\int_{\partial e_i}\vec{\boldsymbol{F}}\cdot\boldsymbol{n}w_l d\partial e_i-\int_{e_i}\vec{\boldsymbol{F}}\cdot\nabla w_l de_i=\int_{e_i}\boldsymbol{S}w_l de_i,\quad l=0,1,\ldots.M,\ \forall w_l,\phi_m\in L^2(\Omega),\quad t\in[0,T], \tag{5}$$

where $\boldsymbol{n}$ represents the outward unit normal vector out of the element at the boundaries.

Communication between the elements in the DG-SEM formulation is achieved through the interface numerical flux. The HLL numerical flux [10] adopted in this paper is as follows:

$$\vec{\boldsymbol{F}}=\begin{cases}\boldsymbol{F}(\boldsymbol{U}_-) & 0\le S_L,\\ \dfrac{S_R\boldsymbol{F}(\boldsymbol{U}_-)-S_L\boldsymbol{F}(\boldsymbol{U}_+)+S_LS_R(\boldsymbol{U}_+-\boldsymbol{U}_-)}{S_R-S_L} & S_L\le 0\le S_R,\\ \boldsymbol{F}(\boldsymbol{U}_+) & 0\ge S_R,\end{cases} \tag{6}$$

where c_0 is the speed of sound， S_L， S_R are the wave speeds on the left and right of the interface, respectively. $S_L=\max(u\pm c_0)$， $S_R=\min(u\pm c_0)$。

Then substitute basis functions and numerical flux back in Eq.(4) to get the semi-discretization system:

$$\frac{d}{dt}\int_{e_i}\boldsymbol{U}_h w_l d\Omega+\int_{\partial e_i}\boldsymbol{F}(\boldsymbol{U}_-,\boldsymbol{U}_+)w_l d\boldsymbol{s}-\int_{e_i}\vec{\boldsymbol{F}}\nabla w_l d\Omega=\int_{e_i}\boldsymbol{S}w_l d\Omega,\quad l=0,1,\ldots.M,\ \forall w_l,\phi_m\in L^2(\Omega),\quad t\in[0,T]. \tag{7}$$

The classical fourth order Runge-Kutta method is applied in time marching. And in order to suppress the spurious waves which are generated by truncating the unbounded domain, the characteristic absorbing boundary condition [11] is adopted too. This also would lead to a significant reduction in computational cost, especially for the three-dimensional large-scale numerical simulation.

3. Results and discussion

3.1 Isentropic vortex case for numerical convergence studies

A convected isentropic vortex propagation problem [12] in the inviscid flow is computed with three different meshes to investigate the convergence property of the proposed method. The background flow is $\{\rho_0,u_0,v_0,p_0\}=\{1,1,1,1\}$. And the initial condition is a linear superposition of a homogeneous background flow field and an isentropic vortex: $\{\rho,u,v,p\}=\{1+\delta\rho,1+\delta u,1+\delta v,1+\delta p\}$. These isentropic vortex perturbations (no perturbation in entropy) are given by (density, pressure and static temperature in a non-dimensional form):

$$
\begin{aligned}
&\delta S = 0, \\
&\delta \rho = \left(1+\delta T\right)^{\frac{1}{\gamma-1}} - 1, \\
&\begin{pmatrix} \delta u \\ \delta v \end{pmatrix} = \frac{\varepsilon}{2\pi} e^{\frac{1-r^2}{2}} \begin{pmatrix} -\left(y-5\right) \\ \left(x-5\right) \end{pmatrix}, \\
&\delta T = -\frac{\left(\gamma-1\right)\varepsilon^2}{8\gamma\pi^2} e^{1-r^2}, \\
&\delta p = \left(1+\delta T\right)^{\frac{\gamma}{\gamma-1}} - 1,
\end{aligned}
\tag{8}
$$

where $r^2 = \left(x-5\right)^2 + \left(y-5\right)^2$， the vortex strength is ε=5, and for air $\gamma = 1.4$.

The numerical computations are performed in the domain $\Omega = [0,10] \times [0,10]$. The time step chosen was small enough so that the temporal error can be negligible. In addition, the periodic boundary conditions were imposed on the boundaries. The exact solution of the LEE with the above initial conditions is just the passive convection of the isentropic vortex along the positive diagonal axis.

Table 1: Accuracy on the isentropic vortex test case at t=10

Order of accuracy	Mesh	L_2 error	L_2 order	L_∞ error	L_∞ order
3	10×10	8.78E-03	—	2.28E-02	—
	20×20	1.96E-03	2.16	4.00E-03	2.51
	40×40	2.50E-04	2.97	5.15E-04	2.96
	80×80	3.27E-05	2.93	6.43E-05	3.00
4	10×10	4.03E-03	—	8.00E-03	—
	20×20	2.16E-04	4.22	5.52E-04	3.86
	40×40	1.74E-05	3.63	5.52E-05	3.32
	80×80	1.16E-06	3.91	4.31E-06	3.68

The accuracy results at t=10 for different order of accuracy and mesh (structured squares elements) are given in Table 1. The numerical results showed that the DG-SEM has achieved the desired order of accuracy except the third order scheme on relatively sparse mesh. The numerical order of accuracy can be defined as below expression:

$$
O = \frac{ln\left(\left\|E_m\right\| / \left\|E_n\right\|\right)}{ln\left(h_m / h_n\right)},
\tag{9}
$$

where $\left\|E_m\right\|$、$\left\|E_n\right\|$ are the some kind of error norm between numerical results with analytical results, respectively. h_m, h_n are the grid scales on the different meshes.

Moreover, in order to investigate the convergence property of this case, we applied three different grid system: a structured squares mesh with 400 elements, a structured triangle mesh with 392 elements and an unstructured triangle mesh with 374 elements, which are all generated by Gmsh [13], an open-source finite element grid software. L_2 error convergence curves for different mesh are presented in Fig. 1. As can be seen from the Fig. 1(a), Fig. 1(b) and Fig. 1(c), the exponential convergence can be obtained for a fixed mesh with increasing local polynomial order, then the error almost remained stable after polynomial order reached a certain value, suggesting that due to the round-off error, the calculations reached machine error levels. Besides, if we ignore the small discrepancies of element numbers between structured squares mesh and triangle mesh, It can also be indicated that the structured squares mesh can obtain a faster convergence than the other two meshes in this case. Fig. 1(d) shows the arithmetic convergence (*h* refinement) and the exponential convergence (*p* refinement) of the DG-SEM.

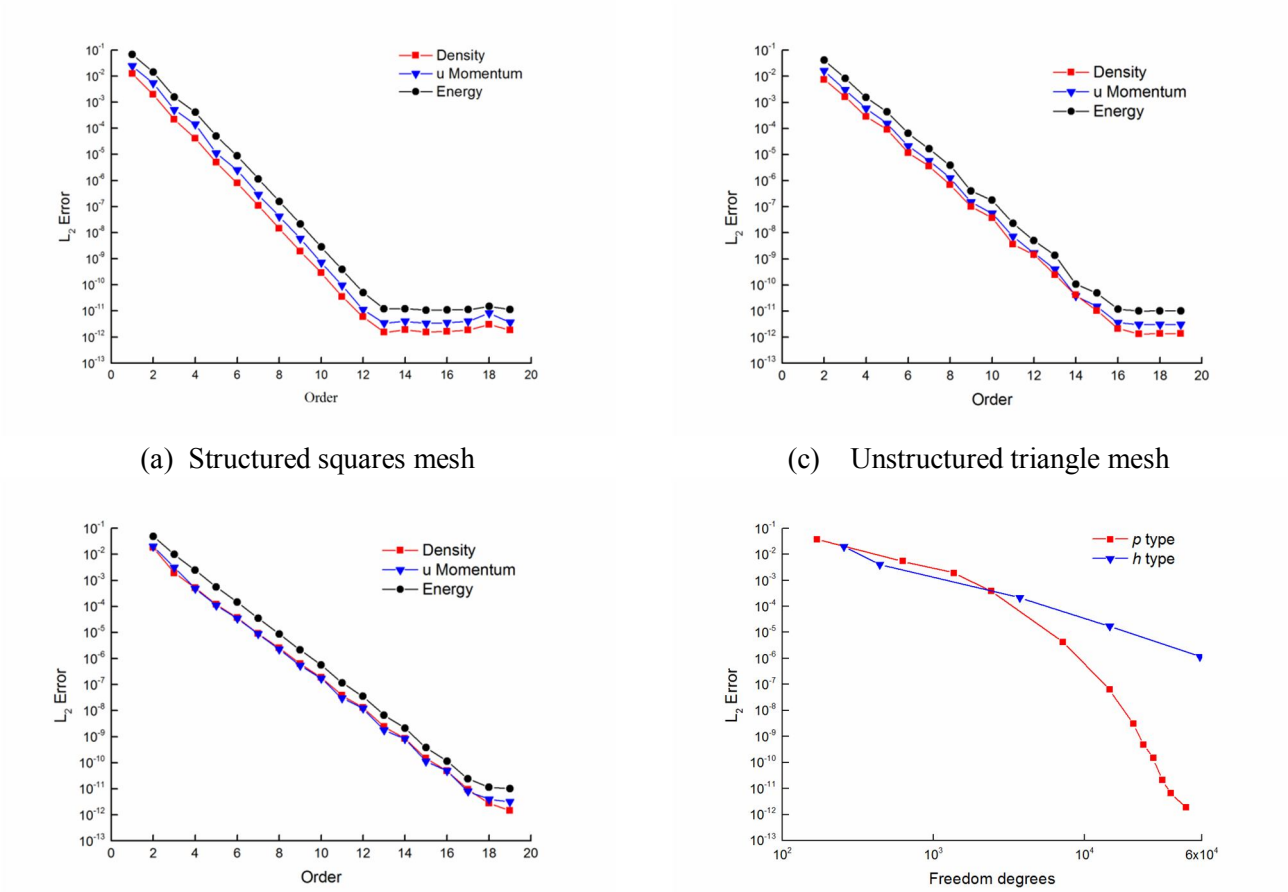

(a) Structured squares mesh

(c) Unstructured triangle mesh

(b) Structured triangle mesh

(d) p and h convergence

Figure 1: L_2 error convergence curves for different meshes.

3.2 Acoustic wave scatting by a circular cylinder

The acoustic wave scatting problem from the Second CAA workshop [14] is a simplified model in which the sound field generated by a propeller is scattered off by the fuselage of an aircraft. The computational domain and the element mesh are shown in Fig. 2. 1830 unstructured triangle elements and a time step $\Delta t = 0.005$ are used. A circular cylinder with radius r = 0.5 is located at the origin. The three monitoring points are: A (r=5, θ=90^0), B (r=5, θ=135^0) and C (r=5, θ=180^0), respectively. In this study the characteristic absorbing boundary condition is also applied to suppress the spurious waves, which are generated by truncating the unbounded domain. The Gaussian pressure pulse at (x, y) = (4,0) is given by the initial condition.

$$p = exp\left[-ln(2)\left(\frac{(x-4)^2 + y^2}{(0.2)^2}\right)\right] \tag{10}$$

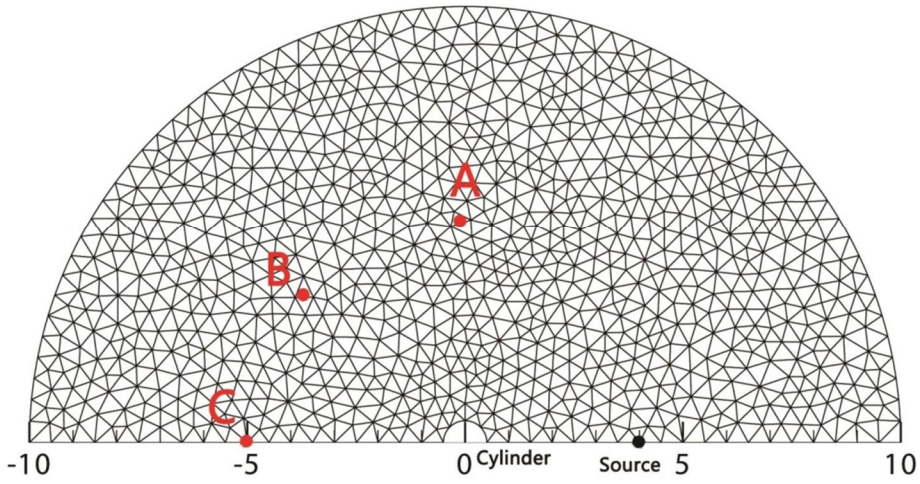

Figure 2: Element mesh for acoustic wave scatting by a circular cylinder.

The instantaneous snapshots of the acoustic pressure perturbation at the time t=2,4,6,8 are shown in Fig. 3. The reflected wave and deflected wave are also captured when the wave front passes through the cylinder surface. As can be seen from the below graph, the acoustic pulse has already reached the out boundary at the time t=8, it can be indicated that the absorbing boundary condition worked well for wave propagation in unbounded domains. Comparison in time of the exact results of pressure with computed results at the three different monitoring points are illustrated in Fig. 4. Numerical solutions are in good agreement with the analytical solutions. As a result of wave reflection and diffraction, the amplitude of acoustic pressure at point B and C are lower than the point A.

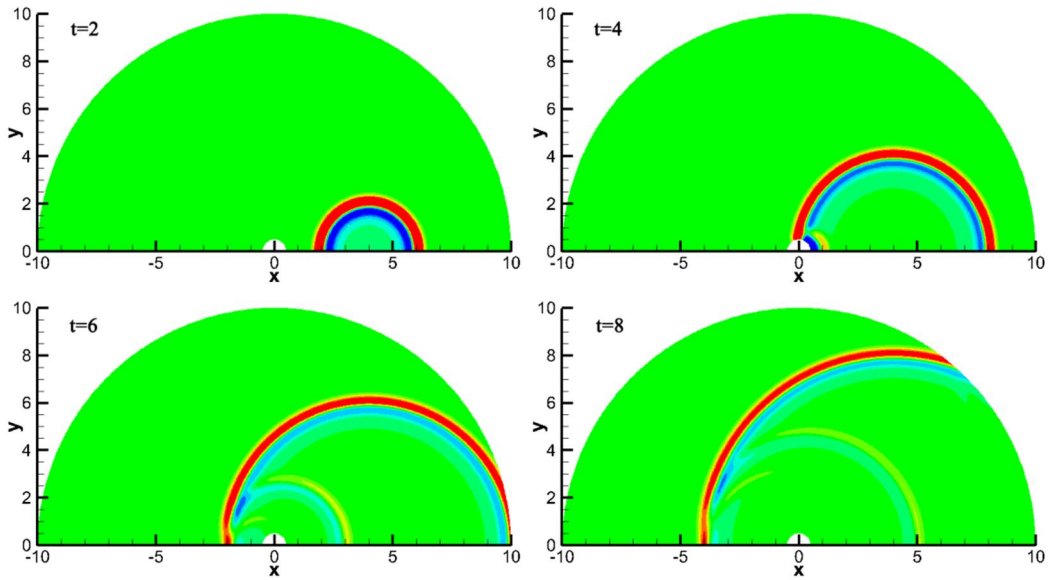

Figure 3: contoursaneous pressure contoures of acoustic wave scattered by a circular cylinder. (10 contour levels between -0.04 and 0.04)

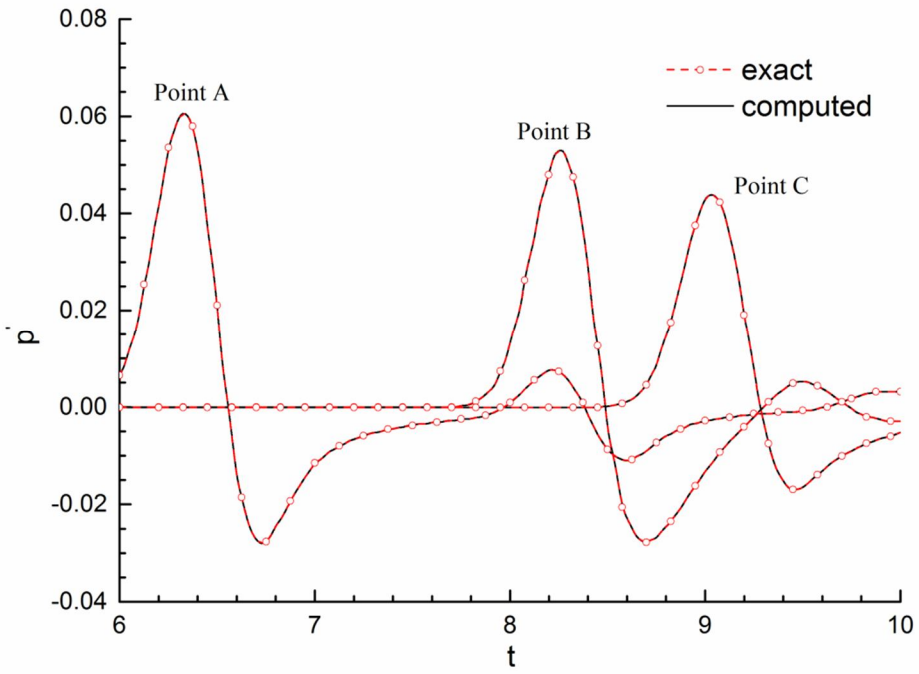

Figure 4: Comparison in time of exact results of pressure with computed results at the three different monitoring points.

4. Conclusions

In the present study, the capabilities of the DG-SEM for the accurate simulation of the acoustic propagation problems using the linearized Euler equation were investigated. The numerical accuracies are verified by the case of a convected isentropic vortex, and the results showed that the DG-SEM can be used for numerical computation with high resolution, due to its properties of exponential convergence. Furthermore, we applied the DG-SEM to solve the case of acoustic wave scatting by a circular cylinder on unstructured triangle mesh. Compared with the available exact results demonstrated the accuracy and flexibility on complex geometries. Future work will investigate the flow-induced noise problems by hybrid methodology with the DG-SEM.

REFERENCES

[1] Li, Xiaodong., Jiang, Min., Gao, Junhui., Lin, Dakai., Liu, Li., and Li, Xiaoyan. Recent advances of computational aeroacoustics, *Applied Mathematics and Mechanics*, **36** (1), 131-140, (2015).

[2] Lele, S. K., Nichols, J. W. A second golden age of aeroacoustics, *Philosophical Transactions of the Royal Society of London A: Mathematical, Physical and Engineering Sciences*, **372** (2022), 20130321, (2014).

[3] Peake, N., and Parry, A. B. Modern Challenges Facing Turbomachinery Aeroacoustics, *Annual Review of Fluid Mechanics*, **44** (1), 227-248, (2012).

[4] Andrea, D. B., Thomas, B., David, F., Hannes, F., Gregor, J. G., Florian, H., and Claus-Dieter, M. High-order discontinuous Galerkin spectral element methods for transitional and turbulent flow simulations, *International journal for numerical methods in fluids*, **76** (8), 522-548,

(2014).
[5] Gassner, G., and Kopriva, D. A. A comparison of the dispersion and dissipation errors of Gauss and Gauss–Lobatto discontinuous Galerkin spectral element methods, *SIAM Journal on Scientific Computing*, **33** (5), 2560-2579, (2011).
[6] Cockburn, B., Karniadakis, G. E., Shu, C. W. The development of discontinuous Galerkin methods, *In discontinuous Galerkin methods*, Springer Berlin Heidelberg, Berlin, (2000).
[7] Karniadakis, G., and Sherwin, S. Spectral/hp element methods for computational fluid dynamics, Oxford University Press, (2013).
[8] Atak, M., Beck, A., Bolemann, T., Flad, D. G., Frank, H., and Munz, C. D. High fidelity scale-resolving computational fluid dynamics using the high order discontinuous Galerkin spectral element Method, *High Performance Computing in Science and Engineering*, Springer International Publishing, Switzerland, 511-530, (2016).
[9] Flad, D. G., Frank, H. M., and Beck, A. D. A discontinuous Galerkin spectral element method for the direct numerical simulation of aeroacoustics, *20th AIAA/CEAS Aeroacoustics Conference*, Atlanta, GA: American Institute of Aeronautics and Astronautics, 2014-2740, (2014).
[10] Qiu, J., Khoo, B. C., and Shu, C. W. A numerical study for the performance of the Runge–Kutta discontinuous Galerkin method based on different numerical fluxes, *Journal of Computational Physics*, **212** (2), 540-565, (2006).
[11] Kim, J. W., and Lee, D. J. Generalized characteristic boundary conditions for computational aeroacoustics, *AIAA Journal*, **38** (11), 2040-2049, (2000).
[12] Dumbser, M., Balsara, D. S., Toro, E. F., and Munz, C. D. A unified framework for the construction of one-step finite volume and discontinuous Galerkin schemes on unstructured meshes, *Journal of Computational Physics*, **227** (18), 8209-8253, (2008).
[13] Geuzaine, C., and Remacle, J. F. Gmsh: a 3-D finite element mesh generator with built‐in pre- and post- processing facilities, *International Journal for Numerical Methods in Engineering*, **79** (11), 1309-1331, (2009).
[14] Hardin, J. C., and Tam, C. K. W. Second computational aeroacoustics workshop on benchmark problems, *NASA CP-3352*, (1997).